High order test bench for extreme adaptive optics system optimization

Emmanuel Aller-Carpentier[*,a], Markus Kasper[a], Patrice Martinez[a], Elise Vernet[a], Enrico Fedrigo[a], Christian Soenke[a], Sébastien Tordo[a], Norbert Hubin[a], Christophe Verinaud[d], Simone Esposito[b], Enrico Pinna[b], Alfio Puglisi[b], Andrea Tozzi[b], Fernando Quiros[b], Alastair G. Basden[c], Stephen J. Goodsell[c], Gordon D. Love[c], Richard M. Myers[c]

[a] European Southern Observatory, Adaptive optics Department – Instrumentation Division - Karl Schwarzschild Str. 2 - D-85748 Garching Bei München - Germany

[b] INAF – Osservatorio Astrofisico di Arcetri - Largo Enrico Fermi 5 - I-55125 Firenze – Italy

[c] Durham University - Department of Physics - South Road - Durham DH1 3LE

[d] Laboratoire d'Astrophysique de Grenoble, 414, rue de la piscine – 38041 Grenoble - France

ABSTRACT

High-contrast imagers dedicated to the search for extrasolar planets are currently being developed for the VLT (SPHERE) and Gemini (GPI) observatories. A vital part of such a high-contrast imager is the extreme adaptive optics (XAO) system that very efficiently removes effects of atmospheric turbulence and instrument aberrations. The high order test bench (HOT) implements an XAO system under realistic telescope conditions reproduced by star and turbulence generators. New technological developments (32x32 actuator micro deformable mirror, read-noise free electron multiplying CCD60, SPARTA real time computer) are used to study and compare two potential XAO wave front sensors: The Pyramid- and the Shack-Hartmann wave front sensors. We will describe the overall design of HOT including the sub-systems. We will present the closed loop study results of the behavior of the Shack-Hartmann wave front sensor in terms of linearity, sensitivity to calibration errors, performance and other specific issues.

Keywords: Extreme Adaptive Optics, high angular resolution, Shack-Hartmann, pyramid, wave front sensing, micro deformable mirrors, L3 CCD.

1. INTRODUCTION

Extrasolar planets direct imaging requires contrasts levels between star and planet better than 10^{-6}. To achieve this requirement it is necessary to implement XAO (eXtreme Adaptive Optics) systems in order to work on diffraction limit and coronographs to produce good PSF suppression. Simulations predict good performances but XAO systems still need to be proven. It's why lab experiments are required in order to check the performance predicted, study new technologies and possible limitations which could reduce XAO correction. This information will be used as feedback for the actual high contrast instruments on development (SPHERE or GPI) and the design of the next instruments generation for extreme large telescopes (E-ELT, TMT …).

Several issues should be tested in order to have some experimental feedback. Shack-Hartmann and Pyramid wavefront sensors appear to be suitable to deliver the correction expected from XAO systems but still need to be characterized under realistic conditions. Static and Quasi-static aberrations on the optical path could be a very critical limiting factor. Studies of XAO postfocal systems are required to avoid these possible limitations.
Next generation of AO instruments will work on telescopes using a large adaptive mirror[1] inside the telescope that for high contrast imaging will act as a woofer. Lab experiments using two deformable mirrors (woofer-tweeter concept[1]) will give information about the best control methods to achieve the optimal performance.
Simulations offers several possible suitable coronographs concepts (APLC, FQPM, Lyot, …) but it's needed to check them performance simultaneously with realistic AO systems.

2. SYSTEM OVERVIEW

The High Order Testbench (HOT)[1] implement an XAO system in order to test some of the points mentioned before. Realistic conditions are achieved simulating the VLT pupil (8m) with a F/50 beam and applying different pupil masks. The HOT bench incorporates a turbulence generator with phase screens to simulate real seeing conditions for three cases: low reduced turbulence (0.5", 0.85" seeing) and full kolmogorov turbulence (0.65" seeing).
Two deformable mirrors for WFE correction are integrated on the system. A first deformable mirror (60 bimorph elements) is used to correct the static aberrations of the bench and will work in a second phase of the project as woofer. This mirror is placed on a TTM (Tip tilt mount), so the doformable mirrors do not need to use stroke to correct this modes.The second one is a micro deformable mirror (electrostatic MEMS device) to correct the high order modes of the generated turbulence.

A cube beamsplitter split the optical beam in two channels. A Shack-Hartmann or a pyramid can be chosen on the first channel path for the wave front sensing using the visible wavelengths. On the second channel an IR camera[1-patr] and a coronograph are used to study the scientific image.
All the optical elements and subsystems are installed and aligned checking aspects as: pupil size, conjugate planes, homogeneity illumination and F number. Both mirrors are characterized in terms of voltage-stroke behavior, coupling, IF, defective actuators. The optical quality was checked for different points of the setup. The bimorph mirror was used to reduce the static aberrations in order to be under the specifications, thus a WFE of 50 nm RMS was achieved (measured on the WFS path). The WFS's and the IR path including the IR camera are installed and aligned too.

3. THE HOT SHACK-HARTMANN WAVEFRONT SENSOR

3.1. SHS design concept

The HOT Shack-Hartmann wavefront sensor designed by the University of Durham, is modeled with an input beam from a 8 m class telescope with a 400 m focal length (F/50). The WFS provides a plate scale of 0.5 arcsec/pixel, with 31x31 subapertures, each detected on 4 x 4 pixels of a 24 μm pixel CCD.
The SHS optics are shown in Figure X, and compose of first a collimating lens used to collimate the F/50 input beam. After this, the lenslet array is placed in a position such that it is conjugate with the DM. A couple of lenses are needed as reimaging optics in order to resample the SHS spots onto the CCD at the correct pitch.

There are three constraints witch determine the characteristics of the optical components used. The input beam (F/50), the plate scale (0.5 arcsec/pix) and the sub-aperture pitch must be 4 pixels (96 μm). Commercial components had should be used in order to reduce costs. This added also a limitation on the pitch/focal length combination of the lenslet array. In order to reduce the effects of aberrations it is recommended to use as long focal lengths as possible for the two reimaging lenses (short focal lengths can result in distortions of the pixel grid at the edge of the array). The final optical parameters found to fit the SHS specifications are summarized on table 1.
The detector chosen for the SHS is a 128 x128 pixel electron multiplying CCD Andor iXON L3. This camera is a sub-electronic readout noise at 400 Hz frames rate working under L3 multiplication gain and a maximum readout rate of 10 Mhz. The camera was characterized to be under the specifications, measuring a value of 0.07 e^- rms read noise for the optimum operate mode.

The WFS will also work as a SFSHS (Spatial Filter Shack-Hartmann Wave Front Sensor)[1] adding pinholes with different sizes on the entrance focal plane of the SHS setup. 1.25, 1.5 and 1.8 λ/d are foreseen to study the performance of the sensor. In addition. a pinhole covering the full 2 arcseconds subaperture will be use on the normal SHS operation to reduce the crosstalk between subapertures.

3.2. SHS alignment

The SHS setup is placed on a linear rail, allowing easy z position adjustment of the optical components. To avoid possible aberrations on the setup the folder mirror that redirect the f/50 beam on the SHS setup was accurately positioned in order to send the beam at the correct high (15 cm) and parallel to the rail.

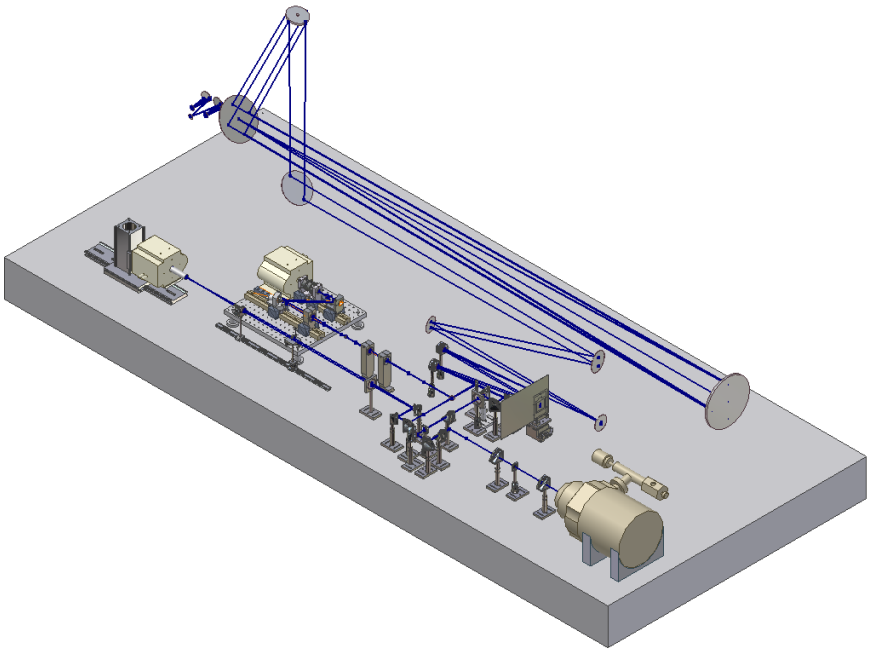

SHS PARAMETERS

Input beam: f/48
Plate scale: 0.52 arcsec/pix
Collimator:
focal length = 450 mm
Reimaging lens 1:
focal length = 250 mm
Reimaging lens 2:
focal length = 80 mm
Lenslet array:
focal length: 35 mm
pitch: 0.3 mm
CCD:
Pixel size: 24 μm

Fig. 1. Schematic HOT setup overview including the SHWS, PWS and the IR path. Table 1. SHS practical optical parameters.

The first collimator lens is installed at the theoretical distance. To find the correct position of the lens, the defocus of the collimated beam is measured using a HASO 64 Shack-Hartmann sensor. The lens is displaced on the rail until we do not measured defocus on the HASO, so a good collimation is assured.
Second step consist on finding the pupil plane where the LA will be placed. For this a compact CCD camera is mounted on the rail. The pupil plane position appears as the plane where the pupil mask is more defined on the compact camera. After this the CCD camera is set at the theoretical distance on the rail. The second reimaging lens is installed on a tube mounted joined to the CCD letting a fine z movement. On the collimated beam, without other optics, the lens should focalize the beam on the CCD camera if the distance between the CCD and the lens is exactly its focal length. We find the optimal position when the PSF is better focalized.

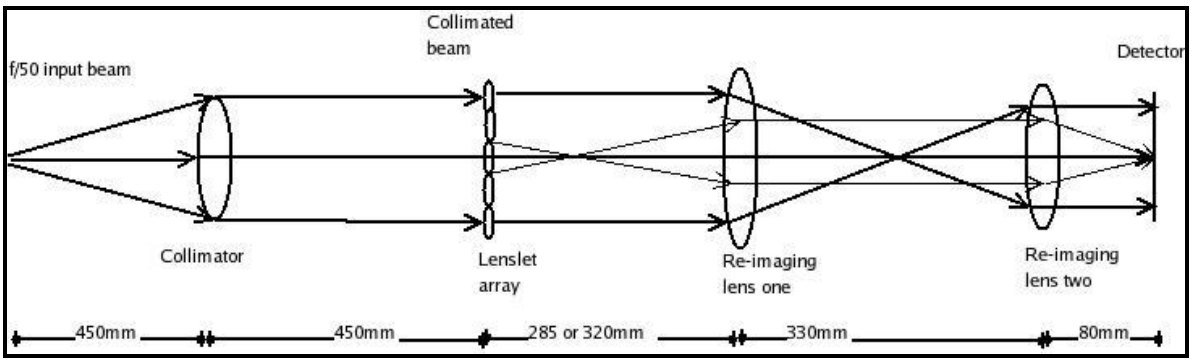

Fig. 2. Schematic SHS HOT setup design.

The first reimaging lens is positioned in order to match the focal planes of both reimaging lenses. This lens is installed on a mound with X and Y accurate movement. Finally the lenslet array is set on the pupil plane found before. The LA is installed on a mount with tip-tilt movement for positioning the LA perpendicular to the beam, rotation movement to avoid rotation between ccd pixels and subapertures and X and Y movement to match subapertures and actuators on the correct Fried geometry.
Once all the optical components are set on the rail an accurate alignment is required. We check that the pupil is centered on the CCD. We centered the subapertures centroids on the CCD until having an homogeneous illuminated group of 4 pixels for each subaperture using the X and Y movements of the first reimaging lens. Then we remove the rotation between CCD and LA rotating this last one. These steps were done visually and using a piece of matlab code that plots on real time the slopes map from the SHS (see next section). The position of the second reimaging lens is readjust. The goal is to find the correct position that reduces the size of the centroids having maximum light on the central pixels and minimum on the external ones.

Finally the position of the subapertures with respect to the BMM actuators is adjusted. The centering of the pupil on the BMM was done previously on the HOT setup alignment. For this we used a group of pushed actuators centered on the BMM showing the position of the pupil respect the BMM. Now this group of actuators is used again to match the position of the subapertures with the actuators. This alignment method is done iteratively until finding an optimal alignment. A magnification around 1.03 is found between subapertures size and actuators pitch.
On the SHS entrance focal plane a magnetic mount is installed. Thus, it is possible to install on this point the spatial filter and a reference fiber. This fiber will be used to acquire reference slopes measurements of the SHS setup in order to not take them in account on the close loop and also permits to verify the quality and stability of the alignment.

3.3. Slope reconstruction.

The SHS HOT slope acquisition is based on a C software WPU emulation (Wave front Processing Unit) implement by the SPARTA group of the ESO. The WPU Server process acquires continuously the pixels from the fiber serial FPDP and process them to compute the gradients (with a simplified algorithm). The slopes are acquired on real time (around 100 Hrz) by MATLAB using a set of MEX functions that acts as bridge between the C and the standard MATLAB code. Thus, the slopes are easily available for the analysis and close loop implementation. The original idea was to use finally a real hardware WPU using FPGA processing, but this possibility continue under study.
WEITHS

4. CONTROL SYSTEM

4.1. BMM characteristics and control.

The control method presented for the SHS required the knowledge of the DM influence functions and the voltage-stroke behavior. The micro deformable mirror is an electrostatic MEMS device from Boston Micromachines. It is a 10.8 mm squared deformable mirror with 340 μm actuator pitch for a total of 32x32 actuators.
The measured mechanical stroke is 1.53 μm PTV (0.83 μm for the interactuator stroke) and 11% of coupling between actuators. The stroke versus voltage for an electrostatic actuators do not follow a linear relation, instead, it could be approximated by a quadratic law[1]. Measuring the stroke-voltage curve this behavior was observed, and it was also found the anomalous behavior predict by the theory at high voltages. Thus, the effective voltage range is 165 volt with a bias value of 114 volts.
The influence functions for all the actuators were measured with a FISBA interferometer. There are 2 inactive actuators inside the pupil (by mirror design) and 4 defective actuators. The lasts are not an important limitation since they are linked and could float with the rest. Instead, the two inactive actuators, placed on the edge of the pupil could be a constraint. A modification on the pupil mask shape was done to hide the area of the two inactive actuators (even if some active actuators are hided too).

The electronics to drive the micro-DM have been produced by Shaktiware. Besides commanding the MEMS1024, Shaktiware also provided a small electronics box that can command the MACAO TTM with ±10V. The corrective drive electronics (CODE) is accessible by TCP connection throw two main links. House-keeping ling (HKL), a non real time communication (configure the CODE, inquire status) and high-speed data link (HSDL), the real-time, low latency data link on which the real-time control commands are sent to the CODE.
The BBM control is easily programmable on MATLAB, since it incorporate a package for TCP connection. Thus, the RTC can be implemented under MATLAB since both slopes acquisition and TTM and BMM are accessible. The RTC implements a square control for the mirror. The RTC computes always displacement positions and in the moment the commands are sent to the mirror, a set of functions convert the displacement values to voltage units following a simple square law. The delay caused by this additional operation was measured to be negligible. This approximation allowed simplifying the control since the square behavior is transparent and makes easier operations as the calibration.

4.2. Modal control implementation.

The modal control follows the PUEO method inspired from Gendron & Lena, 1994[1]. The method consist on obtain the reconstructor as a combination of a zonal interaction matrix and a modal base. The reconstructor is defined as:

$$R^{-1} = B \cdot G \cdot B^{-1} \cdot D^{+}$$
$$\vec{a} = R\vec{c}$$
$$\vec{c} = D\vec{a}$$
$$\vec{a} = B\vec{m}$$

Where $\vec{a}$ is the actuator vector, $\vec{c}$ the measurement vector (slopes) and $\vec{m}$ is a coefficients mode vector. D is the zonal interaction matrix that goes from actuators two measurements (slopes), B is the modal base matrix (goes from modes space to actuators space). G is a diagonal matrix where the ith element is the gain on the mode i.

There are 718 subapertures illuminated on the SHS. Are not available the subapertures outside the pupil, the central obstruction and 10 more on the pupil side (hidden by the pupil mask too). In the original pupil mask the subapertures corresponding to the spider were bad illuminated. In the actual, the spiders size was reduced, thus, these subapertures are available for the wave front measurement. There are 792 actuators surrounding the subapertures configured. The final number of actuators controlled will increase since an external ring of slaved actuators is added. The subpupils and actuator map is showed on figure 3a.

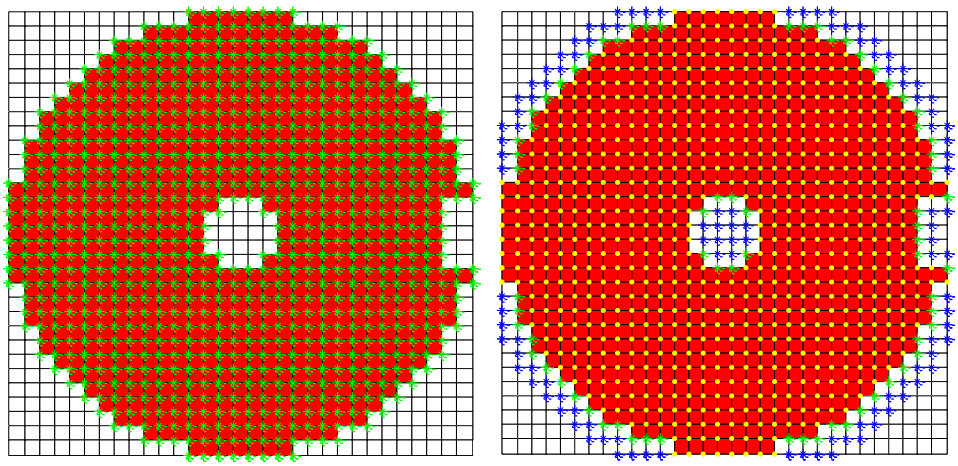

Figure 3. (a) Left: View of the subpupil map, the "asterisco" show the valid actuators. (b) Right: Slaving actuators map. On yellow, normal active actuators, on green, master actuators, and on blue, slaved actuators.

4.2.1. Calibration

A zonal calibration is done but instead of a simple diagonal calibration matrix, we use a Hadamard matrix. This DM actuator pattern is largely demonstrated (Markus et al 2004) to maximize the SNR[1] on the sensor. In other case, the calibration time to obtained similar SNR would be extremely long for a 1024 actuators system. The haddamard matrix apply 1024 voltage patterns, all the actuators are calibrated, and only at the end of the process the active actuators are selected.
In a first step the calibration is done using the same bias voltage for all the actuators (114 volt). The interaction matrix measured is used to close the loop removing static aberrations. Thus, the mirror voltage pattern that minimize the slopes on the SHS are obtained. This pattern is used as bias for a new interaction matrix.
To obtained a good interaction matrix is required to maximized the signal measured on the SHS avoiding saturation on the subapertures. Since the linear range for all the suabepertures were measured previously, it is easy to verify that any of the subapertures is been saturated on the calibration process. Thus, the maximum multiplicative factor for the hadamard modes that avoid saturation on the subapertures is founded. Once obtained the interaction matrix we check that the valid actuators selected previously produce a good signal on the subpupils.

4.2.2. Modal base

The modal base construction is inspired on the method develop by Gendron[1] and applied previously, for example, on the Keck AO, but was never tested for larger actuator AO systems. The idea is to obtain a Karhunen-Loève base where the modes are orthogonal and uncorrelated simultaneously. For this we take on count the space mirror, i.e, the real measured influence functions and the atmospheric profile we want our system to reproduce. Diagonalizing the geometric covariance matrix produces orthogonal modes, and the eigenvectors of the statistical covariance matrix produces uncorrelated modes. Then, a double diagonalization operation of both matrix gives the desiderate base that allows us to go from mode space to actuator space. This modal base avoid the aliasing between modes observed on our system when using a standard a Karhunen-Loève.
The actuators behavior is similar for all the actuators and the only difference is the position on the IF matrix. So, a media IF function is calculated using the information from all the actuators. Then this media IF substitute the individual IF, keeping the position on the IF matrix. Thus, the errors on the IF measurements are eliminated although minor individual actuator information is lost. This media IF matrix is used as input for the modal base reconstruction taking on account only the actuators that produce enough signal on a circular pupil. An atmosphere following a von Karman spectrum with L_0 = 50 m and r_0 = 0.2 m is considered for the computation.

4.3. Slaving

The interactuator stroke is only 0.83 μm. This could be a limitation trying to correct high order modes, since these ones requires higher strokes specially for the actuators on the pupil side and could produce saturation. To solve this problem we consider as actives a ring of actuators just outside the pupil but they will be controlled as slaves of master actuators inside the pupil. Thus, the effective stroke of the master actuator will increase. Some modification on the IM are required since now the slave IF has to be added to the master IF. Also on the control loop the command calculated for the master will be sent to the slaved. The master and slave actuators map is showed on figure 3b.

4.4. Loop control

A simple algorithm is implement for the loop control. Two devices are controlled simultaneously, the TTM and the BMM. The TTM has two channels for tip and tilt correction, so the BMM modal reconstructor do not include this modes. An IM for the TTM is measured on the calibration (in this case actuators and modes commands are equivalent) and the TTM reconstructor is obtained through a simple inversion. The tip and tilt commands are calculated from the WFE measured using this reconstructor. Then we calculate the residual WFE after removing the tip and tilt contribution. Finally, the BMM commands are computed applying the modal reconstructor to the WFE.

5. RESULTS

5.1. SHS characterization

5.1.1. SHS linearity

In order to achieve better performance on close loop it is necessary to know the SHS behaviour on terms of linearity and crosstalk. The TTM is used to obtain the linearity curve of the sensor since we need to produce known variances tilts on the wave front. The two TTM axes will be called channel 0 (Y slopes) and channel 1 (X slopes). Both channels are controlled in the range **-1** to **1**, where 0 is the zero position (it will be called "*normalized units*" (nu)). These values correspond to a voltage range from -10 to 10 volts. Thus, the amplitude of the mount is 500 mas per 0.1 nu. Slopes measurements are acquired for different positions of the useful range of the two TTM axes.
First we check visually on the sensor which is the TTM range necessary to produce a displacement of 1 pix in the centroids position. This value is approximately 0.082 nu, but the slopes measured are around 0.6 pix instead of the 1 pix expected. This is caused by a clearly aliasing between subapertures. To reduced the effect of the crosstalk a pinhole covering covering the full 2 arcseconds subaperture is installed on the focal plane. The mean linearity curves for both cases are showed on figure 4 and the main parameters founded are summarized on table 2.

We can summarize the differences between the cases with and without pinhole as follow:

A) The tilt dynamical range gives the maximal turbulence that the WFS can measure. In both cases it's the same, since this parameter depends on the SHS design (i.e. weights for the slopes calculations).
B) The slopes dynamical range increases a 13%. This parameter depends on the crosstalk between subapertures. Since, by design there is not a guard band between the 4x4 pixels of each subaperture, the sensor suffer from an important crosstalk, the use of the pinhole reduce it clearly.
C) The difference on behavior between subapertures is not important. Only some subapertures in the edge and under the spider present a smaller slope dynamical range. We will need to take care of it when the interaction. matrix acquisition will be determined, so the slope dynamical range map per subaperture calculated is necessary.

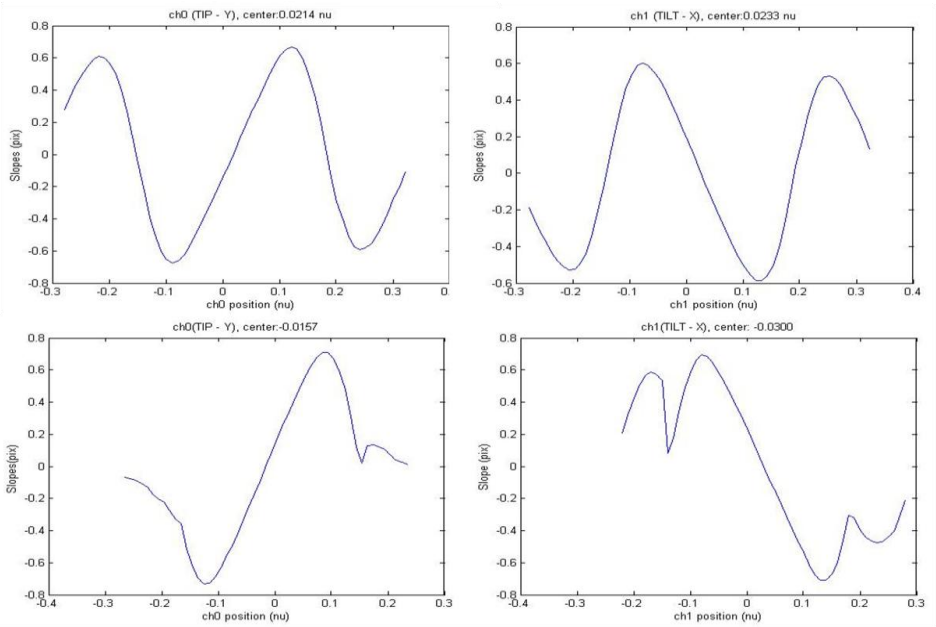

Figure 4. Mean linearity curve on X and Y for the SHS. Up: Without pinhole. Down: with pinhole.

Table 2. SHS linearity parameters.

Without pinhole:

CH0:
max = -0.67 ± 0.08 pix
min = 0.67 ± 0.08 pix;
Dinamical range (tilt) = 0.21 ± 0.01 nu.
Dinamical range (slope) = 1.3 ± 0.1 nu.
Linear range slope: 7.7 pix/nu

CH1:
Max = 0.60 ± 0.08 pix
min = - 0.59 ± 0.09 pix
Dinamical range (tilt)= 0.21 ± 0.01 nu.
dinamical range (slope) = 1.2 ± 0.1 pix.
Linear range slope: 7.1 pix/nu
Mean dynamical range is 1.05 ± 0.05 arsec.

With pinhole:

CH0:
max = 0.73 ± 0.07 pix
min = -0. 75 ± 0.07 pix;
Dinamical range (tilt) = 0.21± 0.01 nu.
Dinamical range (slope) = 1.5 ± 0.1 pix
Linear range slope: 8.1 pix/nu

CH1:
Max = 0.70 ± 0.08 pix
min = - 0.72 ± 0.07 pix
Dinamical range (tilt)=1.4 ± 0.1 nu.
dinamical range (slope) = 0.21± 0.01 nu..
Linear range slope: 7.6 pix/nu
Mean dynamical 1.05 ± 0.05 arsec.

5.1.2. Sensor sensitivity in Fourier space.

The goal is to verify that the sensitivity of the slopes measurements have a well defined dependency with the aberrations spatial frequency *k*. On the SHWFS being a slope sensor, the variance of the measurements is expected to be $\propto k.^2$. This assumes a correction factor[1] $1/\mathrm{dsinc}((dk))^2$ due to the finite sampling with sub-aperture of size d .
The method used consist on building a set of sinusoidal mirror modes on the BMM with 1 to 15 cycles/pupil frequency. We analyze the slope variance measured by the SHS for this set of modes. The curves are shown on figure 5. It show how the first 11 modes have a good adjustment to a square curve. Higher frequencies do not fit since the BMM is not able to well reproduce the modes. If now we take on account the corrective factor, it is show that for the highest modes the adjustment to the curve is better.
On figure 5 it is show the relation between the phase produce by the sinusoidal modes and the field intensity (PSF). As the theory predict, now the field in the focal plane is the unaberrated field due to diffraction plus a series of weighted replications at distances proportional to the frequency. The spatial filter SHS exploits this relationship between the frequency content of the phase aberration and the field intensity and PSF[1].

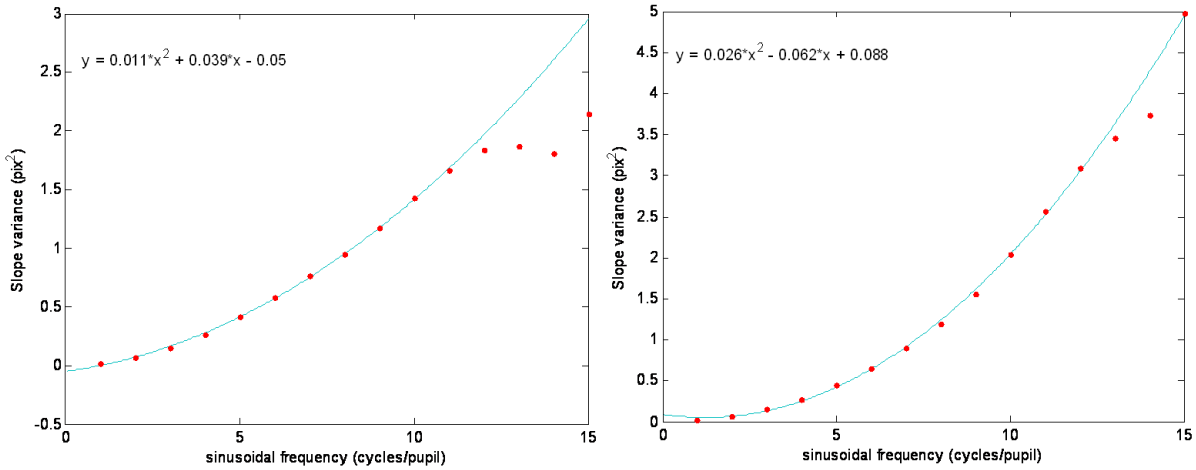

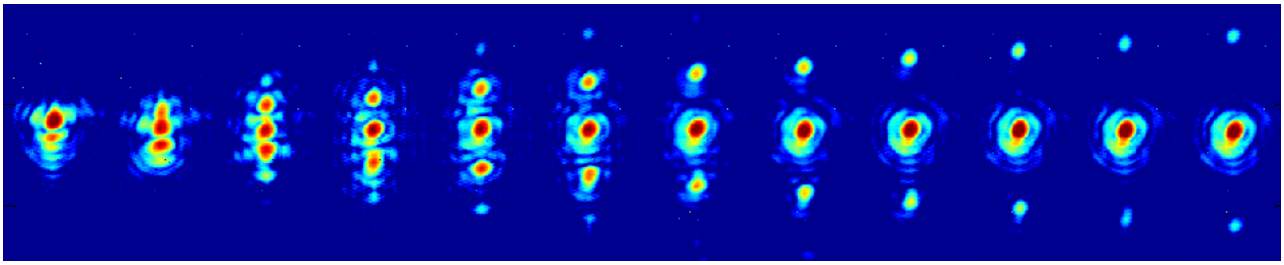

Figure 5. (a) Up: Variance slope study on function of the sinusoidal mode frequency produce by the BMM. On the left adjustment without correction factor applied. On the Right adjustment taking in account the correction factor. (b) down: Focal plane images on the scientific path showing the effect of the sinusoidal modes. Increasing the frequency (1 – 12 cycles/pupil) the psf replications move away from the central PSF. For frequencies 5 and 6, the second order speckle is showed clearly. The images are taken with the IR – ITC camera[1] on band H.

5.2. Phase screen atmospheric behavior characterization with the SHS

The phase screens were characterized previously[1] in terms of spatial resolution with the HASO 64. Now, both were installed on the turbulence generator and the equivalent wind speed was measured on open loop following Conan et all, 1955[1]. The turbulence generator is configured with both phase screens turning on opposite sense at minimum speed. On figure 6a the defocus coefficient spectra is showed. The approximate cut frequency found is around 0.2 Hrz, equivalent to a wind speed of 1.44 m/s for a 8 m pupil. The coherence time of the turbulence was measured computing the temporal autocorrelation of the subapertures. 109 and 188 ms were obtained for the x and y axes respectively.
The atmospheric behavior reproduced by rotating phase screens should follow the Taylor's hypothesis and be considered as "frozen turbulence". Thus, computing the spatiotemporal cross-correlation of the slopes measurements we should see a clear peak crossing the pupil as showed on figure 6b. The wind speed found on this more accurate way is 1.3 m/s. Since only one correlation peak appears implies that the turbulence of both phase screens are superposed with the same direction. If now we repeat the measurements with the phase screen moving in the same direction, two correlation peaks appears, corresponding to the existence of two turbulence layers moving in opposite directions (figure 6(c)).

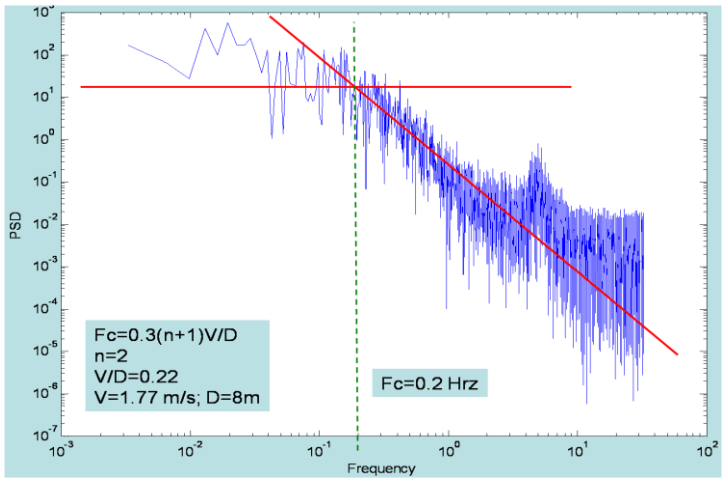

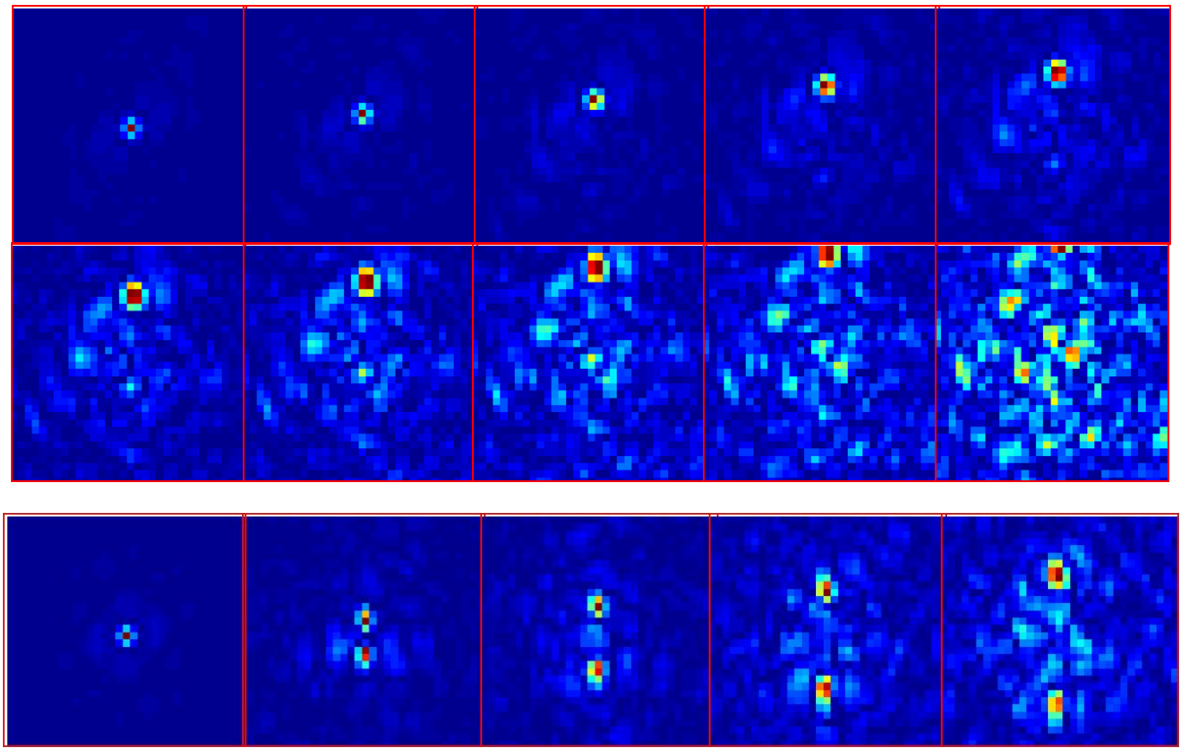

Figure 6(a) Defocus contribution spectra, an aproximate cutoff frequency of 0.2 HZ is founded (b) Series of 10 images representing the spatiotemporal cross-correlation taken 200 ms. A correlation peak is clearly visible and moves uniformely away from the center at a speed 1.3 m/s. Each image show only half of the pupil. (c) Two correlation peaks are visible when we change the sense of the phase screens movement.

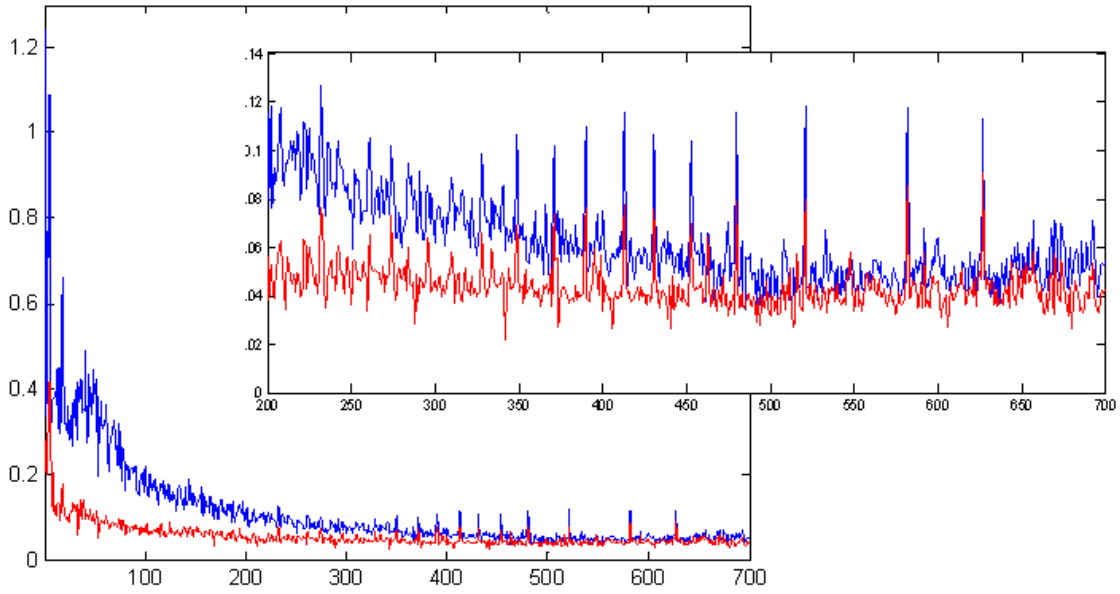

Figure 7. Plot showing the open loop (blue) vs close loop (red) for all the 700 modes (mode vs standard deviation coefficient). In the small plot, zoom on the modes between the 200 and the 700.

5.3. Close loop performance

The SHS close loop use two reconstructors taking on account 400 or 700 modes. Computing the modal coefficients from the residual WFE a clear correction is obtained until mode 400 for both reconstructors (figure 7). On the 700 modes case the last 200 modes are corrected but the correction achieved is smaller.
The turbulence is simulated with the 0.5" seeing phase screens turning at minimum speed. The equivalent wind speed is 1.3 m/s (two layers with same speed and direction) as mentioned before. The close loop works at 50 Hrz, with a measured bandwith of 2.5 Hrz.
The PSF measured is showed On figure 8. 85% SR is achieved on H band using the ESO IR Test Camera (ITC) (The IR path optics quality[1] is equivalent to 95 % SR). On the PSF image, the spots on the top and the bottom are ghosts from the BMM cover window. Since the reflection comes from outside the window they are not corrected by the AO loop.

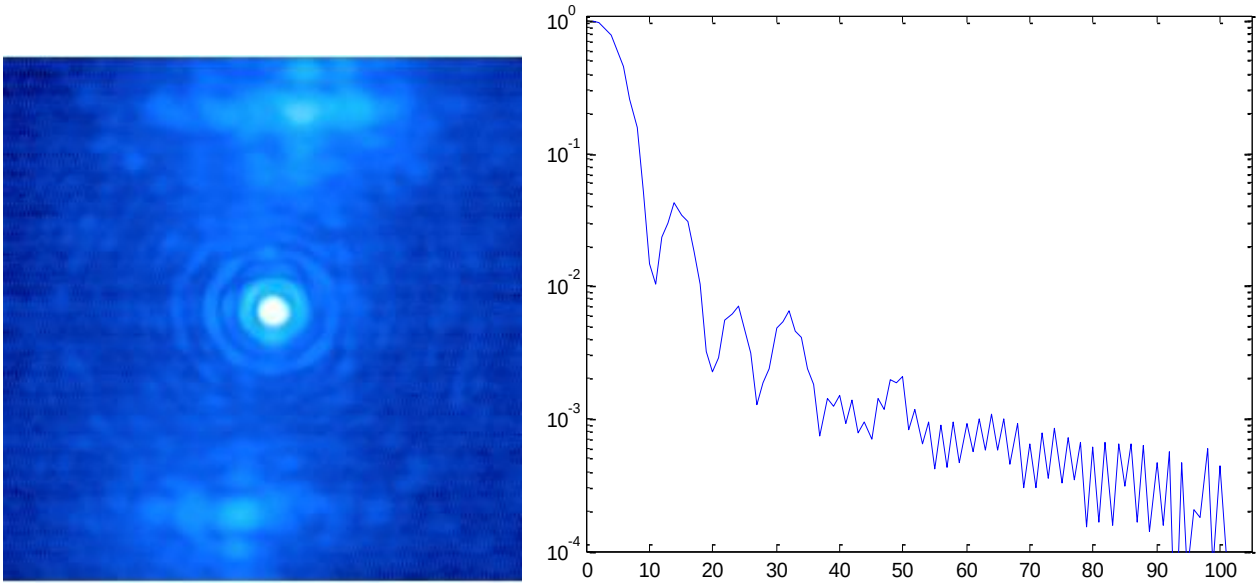

Figure 8. (left) PSF image on H band (85 % SR). (right) Plot of a PSF cut.

Gain matrix

Thierry … sof ….
Size of the central obscuration
Referente to the keck ao method.
UN triple lo de no probado antes

6. CONCLUSIONS AND PERSPECTIVES

Extras:
. The patterns are applied positive and negative and then ponderated to remove static aberrations.